The Astrophysical Journal, 883:43 (8pp), 2019 September 20 https://doi.org/10.3847/1538-4357/ab304c

On the Nature of the Bright Core of Solar Coronal Mass Ejections

H. Q. Song[1], J. Zhang[2], X. Cheng[3], L. P. Li[4], Y. Z. Tang[1], B. Wang[1], R. S. Zheng[1], and Y. Chen[1]
[1] Shandong Provincial Key Laboratory of Optical Astronomy and Solar-Terrestrial Environment, and Institute of Space Sciences, Shandong University, Weihai, Shandong 264209, People's Republic of China; hqsong@sdu.edu.cn
[2] Department of Physics and Astronomy, George Mason University, Fairfax, VA 22030, USA
[3] School of Astronomy and Space Science, Nanjing University, Nanjing, Jiangsu 210093, People's Republic of China
[4] Key Laboratory of Solar Activity, National Astronomical Observatories, Chinese Academy of Sciences, Beijing, 100101, People's Republic of China
Received 2019 April 11; revised 2019 July 3; accepted 2019 July 7; published 2019 September 18

Abstract

Coronal mass ejections (CMEs) often exhibit the classic three-part structure in a coronagraph, i.e., the bright front, dark cavity, and bright core, which are traditionally considered as the manifestations of coronal plasma pileup, magnetic flux rope (MFR), and filament, respectively. However, a recent survey based on 42 CMEs all possessing the three-part structure found that a large majority (69%) do not contain an eruptive filament at the Sun. Therefore, a challenging opinion is proposed and claims that the bright core can also correspond to the MFR, which is supported by the CME simulation. Then what is the nature of the CME core? In this paper, we address this issue through a CME associated with the eruption of a filament-hosting MFR on 2013 September 29. This CME exhibits the three-part morphology in multiple white-light coronagraphs from different perspectives. The new finding is that the bright core contains both a sharp and a fuzzy component. Through tracking the filament motion continuously from its source region to the outer corona, we conclude that the sharp component corresponds to the filament. The fuzzy component is suggested to result from the MFR that supports the filament against the gravity in the corona. Our study can shed more light on the nature of CME cores, and explain the core whether or not the filament is involved with a uniform scenario. The nature of the CME cavity is also discussed.

Key words: Sun: activity – Sun: coronal mass ejections (CMEs) – Sun: filaments, prominences

Supporting material: animations

1. Introduction

Coronal mass ejections (CMEs), one of the most energetic explosive phenomena in the solar atmosphere, can eject a large quantity of plasma and magnetic flux into the interplanetary space (Chen 2011; Webb & Howard 2012), and adversely affect human high-technology systems around the Earth (e.g., Gosling et al. 1991; Webb et al. 1994; Zhang et al. 2003, 2007). Theoretically, it is widely believed that CMEs result from the eruption of magnetic flux ropes (MFRs), which are volumetric current channels with a helical magnetic field wrapping around their central axial field lines. Some numerical simulations (Chen 1996; Lin & Forbes 2000; Lin et al. 2004) and observations (Zhang et al. 2012; Cheng et al. 2013, 2014; Patsourakos et al. 2013; Song et al. 2014b, 2015; Wang et al. 2017; Gou et al. 2019) support that the MFR can exist prior to a solar eruption (dubbed as a seed MFR sometimes) and grow further through magnetic reconnection during the eruption. In the meantime, some other simulations (Mikić & Linker 1994; Antiochos et al. 1999) and observations (Cheng et al. 2011; Song et al. 2014a; Ouyang et al. 2015, 2017) support that the MFR can form from a sheared loop during the eruption, and also grow further through reconnection. Observationally, more than 70% of CMEs are found to be associated with filament eruptions (e.g., Webb & Hundhausen 1987; Gopalswamy et al. 2003). Filaments (also called prominences when observed near the solar limb) are about 100 times cooler and denser than the coronal material (e.g., Yan et al. 2016; Song et al. 2017a). It is generally accepted that the filament is supported against gravity by the MFR that contains magnetic dips in its field lines, i.e., sites where the field lines are locally horizontal and curved upward (Kippenhahn & Schlüer 1957). Therefore, CMEs, MFRs, and filaments are closely correlated to each other.

The observations of white-light coronagraphs demonstrate that ~30% of CMEs have the classic three-part structure, i.e., the bright front (BF), dark cavity (DC), and bright core (Munro et al. 1979; Illing & Hundhausen 1985; Webb & Hundhausen 1987). A recent comprehensive statistical study suggests that at least 40% of CMEs have the MFR structures, including both the two-front and three-part morphologies (Vourlidas et al. 2013). As the brightness in white light coronagraph images is proportional to the electron density, the three-part structure corresponds to a high-low-high density sequence. When the MFR, with filament contained in its trailing part, lifts off from the source region, it will expand and stretch the overlying loops successively (e.g., Chen 2009). The background plasmas will pile up along the MFR front border and evolve into the CME BF (Forbes 2000). Therefore, the three-part structure of CMEs is naturally explained as the manifestations of coronal plasma pileup (high density), MFR (low density), and filament (high density) sequentially.

However, this explanation of the bright core of CMEs has been challenged (Howard et al. 2017; Song et al. 2017b). A survey based on 42 CMEs all with the three-part structure demonstrated that ~69% of them are not associated with any eruptive filament. Howard et al. (2017) speculated that the CME core could be produced by the geometric projection of a twisted MFR, which is supported by their CME simulation. Alternatively, they pointed out that the core can arise spontaneously from the MFR eruption as the density within

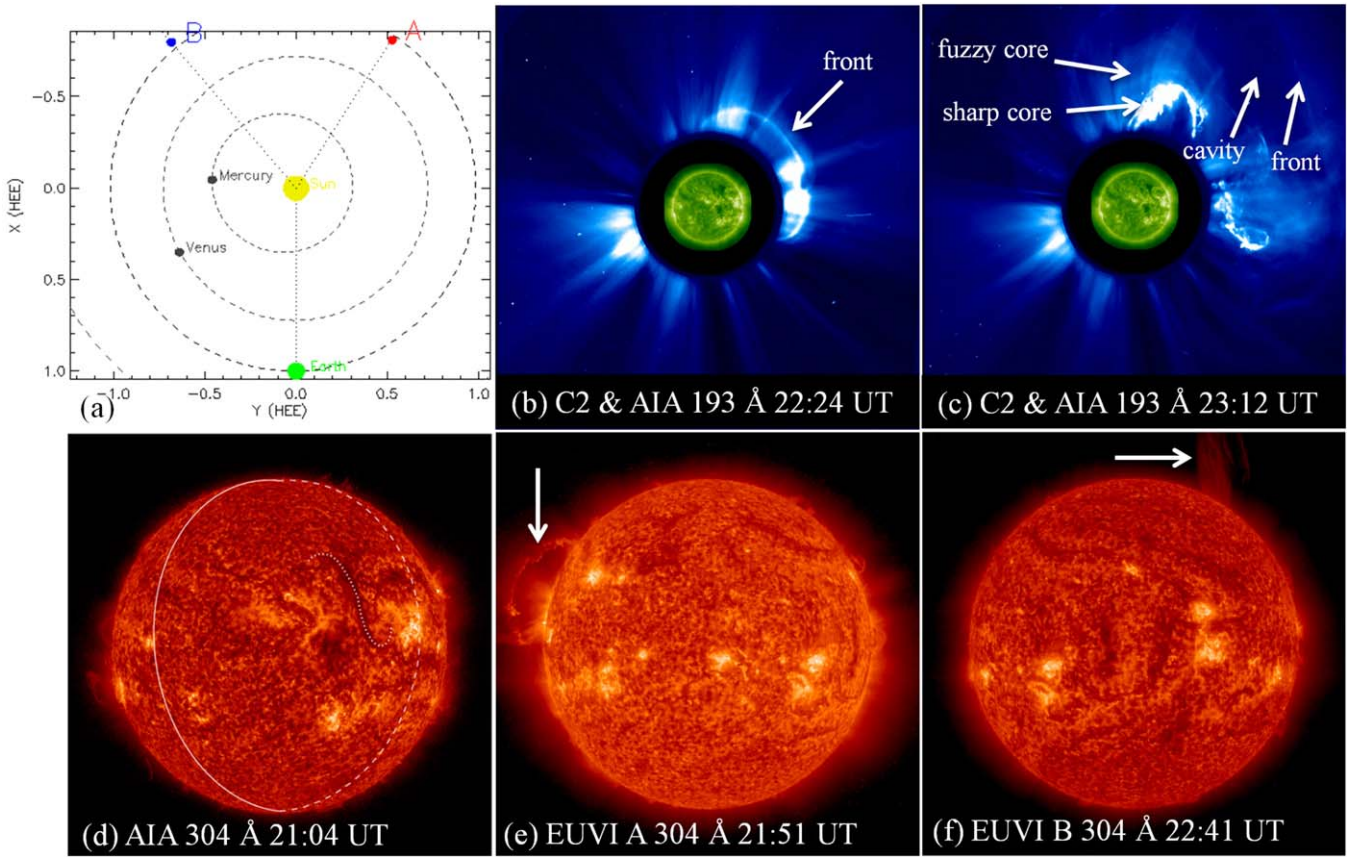

Figure 1. (a) Positions of *STEREO-A/B* and Earth (*SDO/SOHO*) in the ecliptic plane on 2013 September 29 (b) and (c) Composite images of the C2 and AIA 193 Å, which are accompanied by animation (a) that displays the CME eruption continuously from 22:00 UT to 23:48 UT with a duration of 2 s. (d)–(f) 304 Å image of AIA, EUVI A, and EUVI B, respectively. Panels (d)–(f) are accompanied by animation (b) that displays the filament eruption process from 21:21 UT to 22:26 UT with a duration of 4 s.

(Animations (a and b) of this figure are available.)

the MFR increases. Simulations using the catastrophe model (Linker et al. 2001; Lin et al. 2004; Reeves et al. 2010) and the breakout mechanism (Lynch et al. 2004; Zuccarello et al. 2012) have shown the density increase within the MFR. Observations further demonstrated that the bright core corresponds to an erupting MFR through a three-part CME without accompanying filament from both edge-on and face-on perspectives (Song et al. 2017b). Then one question arises naturally: what is the nature of the CME core, and could we observe a core possessing two parts for a filament-related CME if both the MFR and filament can be imaged as the core? In this paper, we address this issue through a CME associated with a filament eruption on 2013 September 29. Instruments and results are presented in Sections 2 and 3, respectively. Section 4 is the discussion, followed by a summary in Section 5.

2. Instruments

The data sets are provided by five instruments, including the Atmospheric Imaging Assembly (AIA; Lemen et al. 2012) on board the *Solar Dynamics Observatory* (*SDO*), the Extreme Ultraviolet Imager (EUVI) and the white-light coronagraphs (COR1 and COR2; Howard et al. 2008) on board the *Solar Terrestrial Relations Observatory* (*STEREO*), and the Large Angle and Spectrometric Coronagraph (LASCO; Brueckner et al. 1995) on board the *Solar and Heliospheric Observatory* (*SOHO*). Both the *SDO* and *SOHO* observe the Sun from the Earth perspective, while *STEREO* consists of twin spacecraft orbiting the Sun, one ahead of (A), and the other behind (B), the Earth. *STEREO-A* and *-B* can provide observations from different perspectives as they separate from the Earth by ∼22° each year in heliocentric longitude.

The AIA images the solar corona with high cadence (12 s), high spatial resolution (0.″6 per pixel), and large field of view (FOV, 1.3 $R_\odot$) in seven EUV passbands. The EUVI provides solar EUV images at four wavelength with an FOV of 1.7 $R_\odot$, partially overlapping with that of COR1 (1.4–4 $R_\odot$), and COR2 has a larger FOV (2–15 $R_\odot$). This enables us to observe the erupted filament continuously from the solar surface to the outer corona. The LASCO also possesses a large FOV covering 2.2–30 $R_\odot$ (C2: 2.2–6 $R_\odot$; C3: 4–30 $R_\odot$), and only C2 is used in this research.

3. Results

A CME was recorded by the *SOHO*, *STEREO-A*, and *STEREO-B* from three perspectives on 2013 September 29 when *STEREO-A (B)* was 147° west (139° east) of the Earth as shown in Figure 1(a). Its BF is recorded clearly at 22:24 UT by the C2 as denoted with the arrow in Figure 1(b). The CME has a linear speed of 1179 km s^{-1} (CDAW: https://cdaw.gsfc.nasa.gov/) and exhibits the three-part structure in the C2 FOV as displayed in Figure 1(c). Its bright core can be distinguished as two parts, one is sharp bright, and the other is fuzzy bright. The BF, DC, sharp,

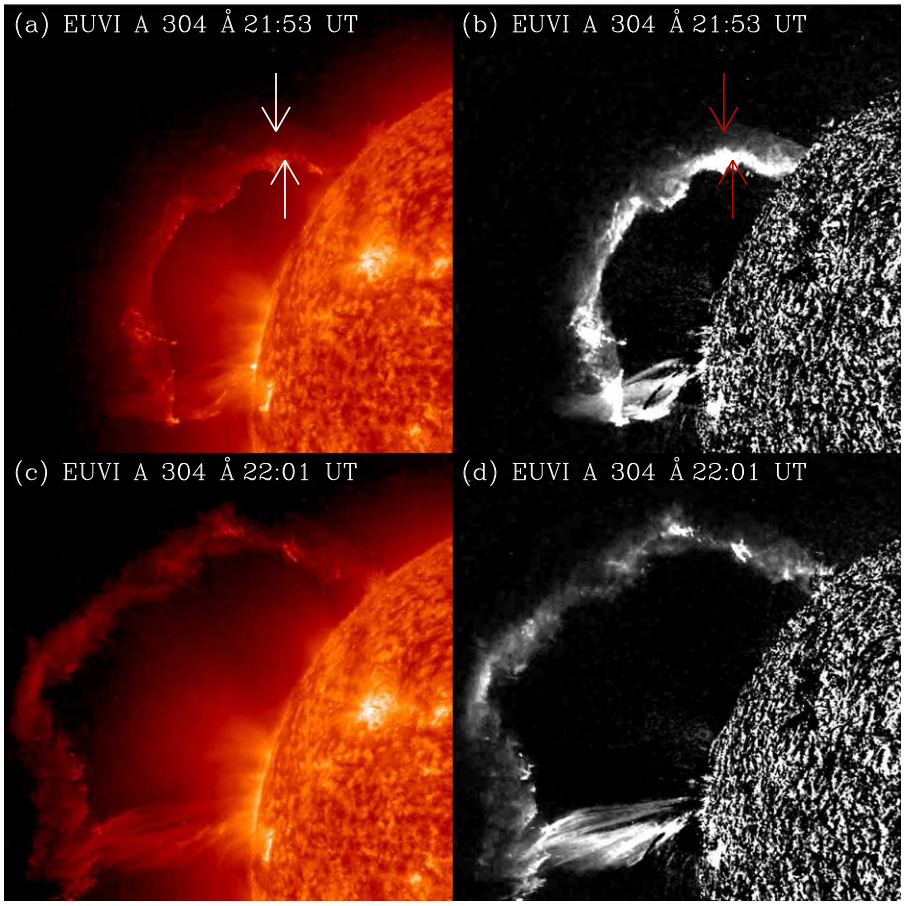

Figure 2. Observations of the filament eruption by the EUVI A. (a) and (c) The direct image of 304 Å. (b) and (d) The base-difference image of 304 Å. This figure is accompanied by an animation that displays the complete eruption process recorded by the EUVI A. The animation starts at 21:28 UT and ends at 22:16 UT with a duration of 3 s.

(An animation of this figure is available.)

and fuzzy cores (FCs) are depicted with the white arrows. See the accompanying animation (a) to inspect the CME continuously. The CME results from the eruption of a quiescent filament that exhibits an inverse-sigmoidal morphology (as delineated by the white dotted line) with its center located at the helographic coordinates of ∼N20W30 from the Earth perspective as presented in the AIA 304 Å image (Figure 1(d)). The white-dashed and solid curves depict the solar limbs observed from *STEREO-A* and *-B*, respectively. It is clear that the filament source region can only be imaged from the Earth perspective, approaching the face-on observation to the filament. The EUVI A/B on board *STEREO-A/B* records the partial eruption process in the 304 Å passband, which is close to the face-on/edge-on perspectives shown in Figures 1(e)/(f), with the arrow pointing to the erupted filament. See the accompanying animation (b) to examine the filament eruption process from three views simultaneously. The animation shows that the EUVI B only records the northern leg of the erupted filament, and the disk observations of AIA 304 Å images display obvious flare-ribbon separation during the eruption, indicating that more poloidal magnetic fluxes are added to circle the filament through magnetic reconnection, i.e., the MFR is growing (e.g., Aulanier et al. 2012; Kazachenko et al. 2017). It is natural to connect the filament with the sharp bright core, because the high-density filament tends to be concentrated (Wood et al. 2016) and exhibits the sharp brightness, obviously discernible from its surroundings. However, the FOV gap between the AIA and LASCO/C2 prevents us from confirming the correspondence, so the *STEREO* data is further analyzed to identify the nature of the sharp core (SC).

Though the filament source region is unobservable for the twin spacecraft of *STEREO*, both EUVI A and B record partial motion of the erupted filament as mentioned. Figure 2(a) presents the EUVI A observation in 304 Å passband at 21:53 UT, which shows a fuzzy bright part (denoted with the downward arrow) ahead of the sharp bright filament (denoted with the upward arrow). To display this feature clearly, the base-difference image is shown in Figure 2(b), where the red arrows mark the two components. The fuzzy part disappears gradually when the filament moves outward as shown in the direct image (Figure 2(c)) and base-difference image (Figure 2(d)) at 22:01 UT, where only the previous sharp part remains obviously. The EUVI-B 304 Å images only display the sharp filament, without the accompanying fuzzy part (not shown here), as the filament enters into its FOV since 22:04 when the fuzzy part is not discernible even in the EUVI A images. The image recorded at 21:26 UT is selected as the base image in both Figures 2(b) and (d). See the accompanying animation to inspect the eruption process. The fuzzy part in 304 Å images should not represent the MFR as its volume does not exhibit an obvious increase during the filament propagation outward. It is possible that the fuzzy part becomes dimmer progressively, partially resulting from the filament approaching

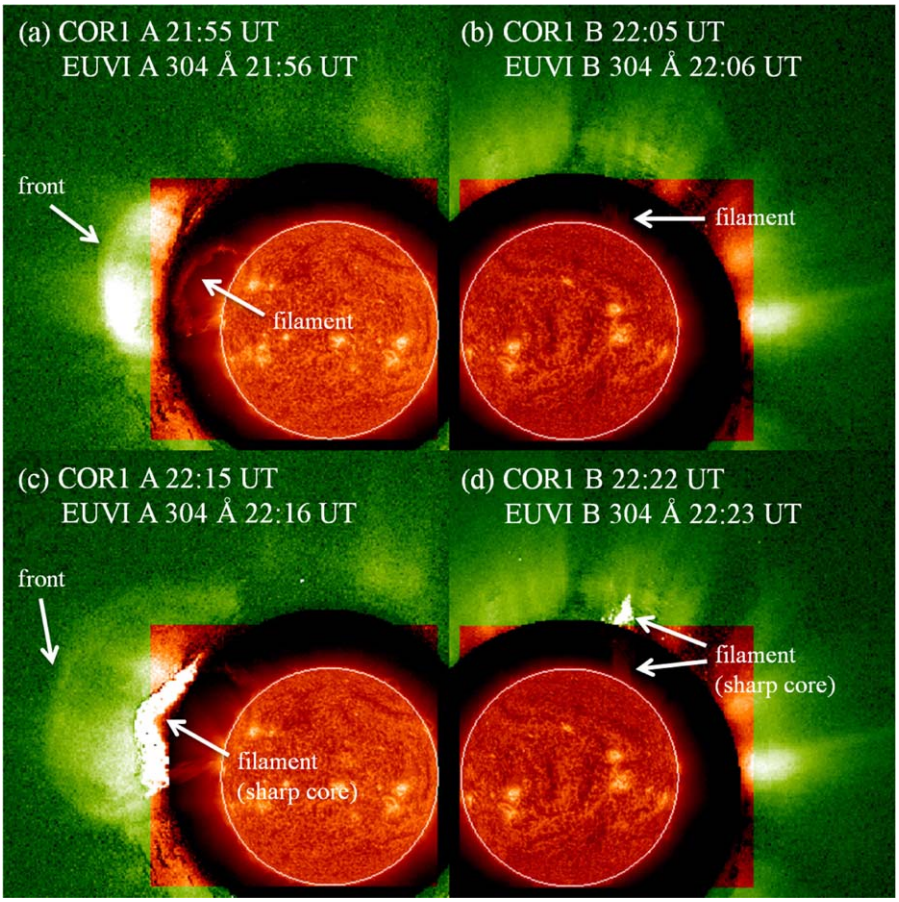

Figure 3. The composite observations of EUVI 304 Å and COR1. Left/right panels are the results provided by *STEREO-A/B*. This figure is accompanied by an animation that displays the complete eruption process from two perspectives and illustrates that the filament corresponds to the sharp bright core. The animation starts at 21:35 UT and ends at 22:17 UT with a duration of 2 s.

(An animation of this figure is available.)

the edge of the EUVI FOV, where the filament can still be visible while the fuzzy structure is not.

Figure 3 displays the composite observations of EUVI 304 Å and COR1. The CME front can be observed in the COR1A FOV at 21:55 UT when the filament has not entered into the COR1 FOV, as shown in Figure 3(a). Therefore, no CME core is observed in the COR1A FOV at this time. At 22:15 UT, the filament ascends to a higher altitude and appears in the COR1A FOV as shown in Figure 3(c), where both the BF and core of the CME can be observed by the COR1A as pointed with the arrows. The observations of *STEREO-B* provide similar results. At 22:06 UT, the northern leg of the filament can be recorded in the EUVI B 304 Å passband (Figure 3(b)), and at 22:22 UT, the filament enters into the COR1B FOV and corresponds to the CME SC as displayed in Figure 3(d). These composite observations unambiguously demonstrate that the erupted filament evolves into the sharp bright core of the CME. See the accompanying animation to examine the correspondence between the filament and the CME core. The FC in C2 observation (Figure 1(c)) is not obvious in the COR1 static images, which might be due to the relatively lower sensitivity of COR1 and/or the projection influence of complex foreground and background structures in the low corona. We will describe the FC mainly through the COR2 observations presented in Figures 4 and 5.

To display both the SC and FC, and further confirm the correspondence between the filament and the SC, the composite images of the EUVI 304 Å, COR1, and COR2 are presented in Figure 4. At 22:39 UT, both the front and core are visible in COR2A FOV as shown in Figure 4(a), where the cyan dots depict the filament front observed with COR1A at 22:37 UT (not shown here) and illustrate that the filament corresponds to the sharp bright core. Only the BF (depicted with blue dots) can be observed by COR2B at this time, as shown in Figure 4(b), because the filament is still blocked by the COR2B occulter. At 22:54 UT, a fuzzy bright core appears in the COR2B FOV, as delineated with the white dashed line in Figure 4(d). This FC does not correspond to the erupted filament because the filament is still blocked by the COR2B occulter at this time. At 23:24 UT, aside from the fuzzy bright core component (delineated with the white dashed line) COR2B records a sharp bright core component as depicted with the cyan dots in Figure 4(f), which corresponds to the northern leg of the erupted filament as delineated with the cyan dots in Figure 4(e). Note that the observational times of the right panels are not shown as they are the same as the left panels. Figure 4(g) presents the pixel intensities along the black dotted line in Figure 4(f), which are normalized to their maximum and clearly exhibit the CME sub-structure, i.e., the SC, FC, DC, and BF. The intensity of the sharp component is significantly larger than that of the fuzzy part and the two core components can be distinguished clearly. It is reasonable to suggest that the fuzzy component/area results from the MFR as it encircles the filament, and previous studies demonstrated that the MFR can correspond

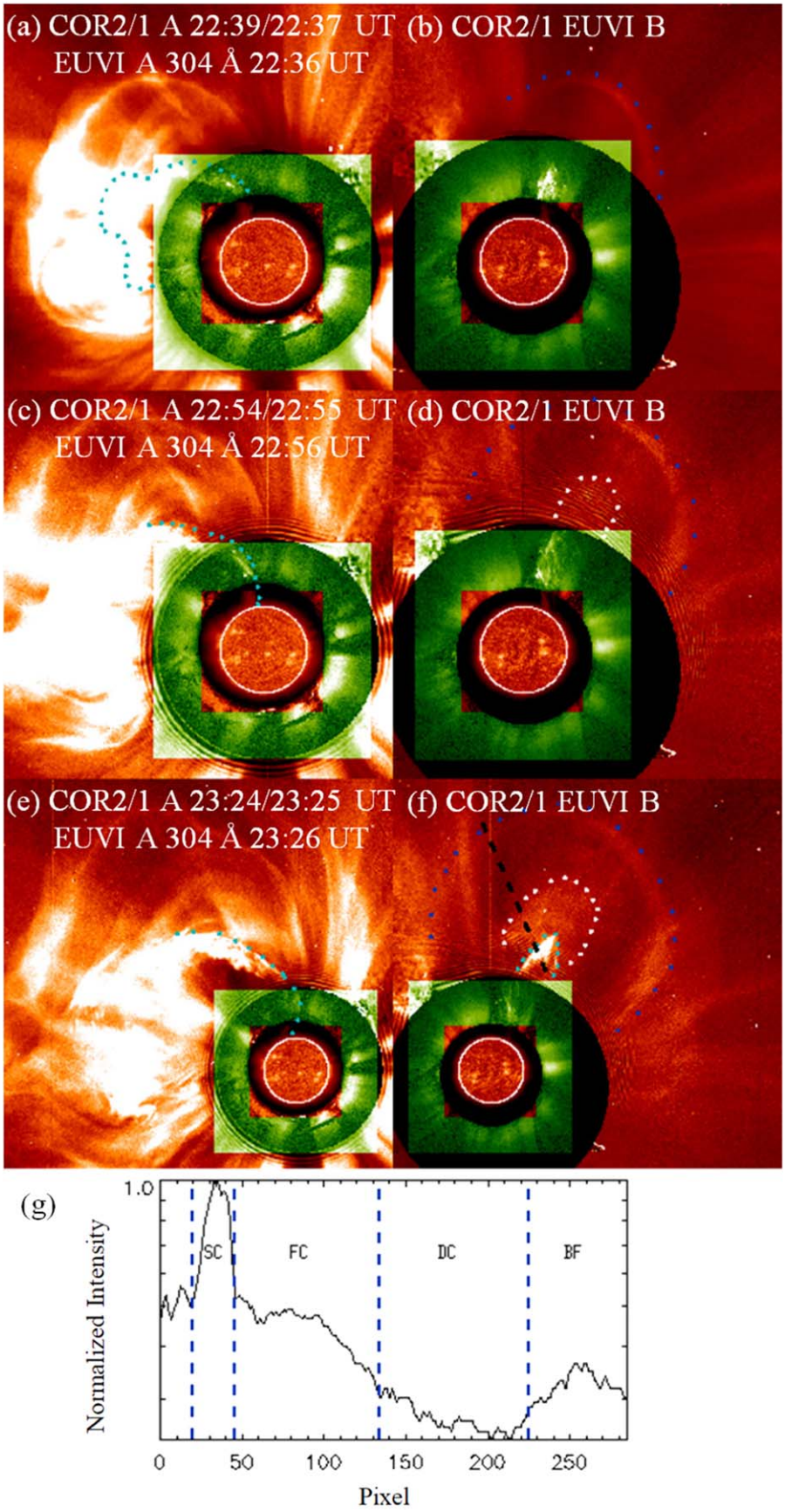

Figure 4. The composite observations of EUVI 304 Å, COR1, and COR2. Left/right panels are the results provided by *STEREO-A/B*. The cyan dots in the left panels and panel (f) depict the filament front, and the blue dots in the right panels depict the CME front. The bottom panel is the normalized intensities along the black dotted line (from bottom to top) in Panel (f). See text for more details.

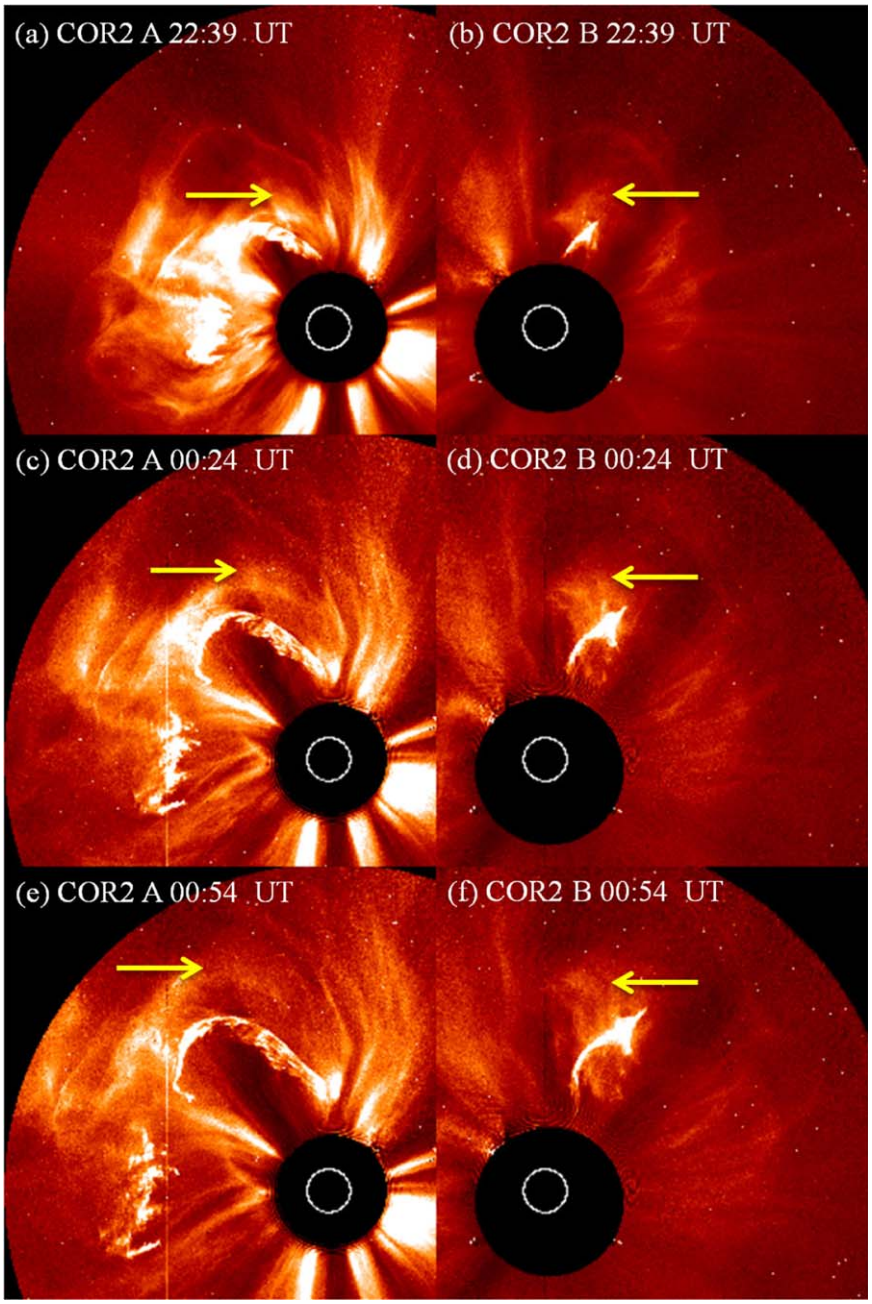

Figure 5. The CME observed through the COR2A (left) and COR2B (right). The white circle in each panel depicts the solar limb. This figure is available as an animation that displays the propagation process continuously from 21:24 UT to 01:24 UT with a duration of 2 s, demonstrating the expansion of the fuzzy core.
(An animation of this figure is available.)

to the CME core (Howard et al. 2017; Song et al. 2017b). The CME morphology is closer to the classic three-part structure in the COR2B FOV as it mainly images the northern CME part. The middle and southern parts of the CME are severely influenced by the writhed filament and interaction between the CME and streamers, which make their three-part structure unclear in the COR2A FOV. The sharp and FC components in the LASCO/C2 FOV (Figure 1(c)) can be understood with the same explanation. It is key to point out that the CME can still exhibit the three-part structure (front, cavity, and FC) if no filament (SC) is involved in this event.

If the FC corresponds to the MFR with higher density and magnetic field relative to the DC, there would be no force/pressure balance between the FC and the cavity and the FC should exhibit expansion, which is observed during its propagation outward by both COR2A and COR2B, as shown in Figure 5. The yellow arrows depict the FC in each panel; we can find that the FC expands with time and possesses larger volume from top to bottom panels, and the filament (SC) keeps concentrate relatively during the process. Similar phenomena have been reported by Song et al. (2017b), which showed that the CME core (i.e., the MFR) exhibits obvious expansion and the spatial extent of the cavity reduces. The original cavity can also be transformed into the MFR shell through magnetic reconnection that occurs in the current sheet behind the CME (Lin et al. 2004). The FC components in Figures 5(b), (d), and (f) should correspond to the fuzzy regions in Figures 5(a), (c), and (e), respectively, as indicated by the arrows.

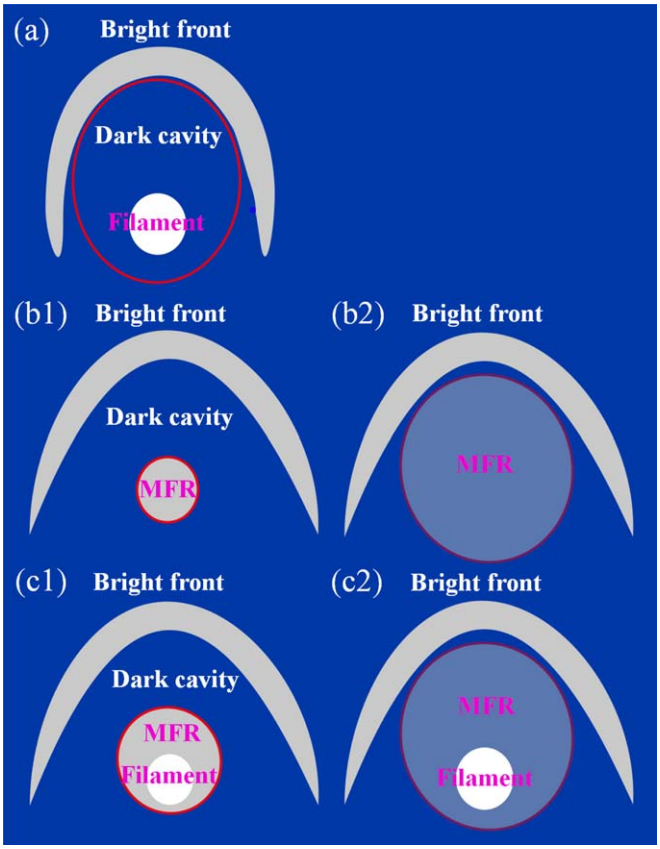

Figure 6. Schematic drawings of the traditional (a) and the challenging (b1), (b2) scenarios to explain the three-part structure of CMEs that are observed edge-on in the white-light coronagraph. (c1), (c2) Our new scenario that can explain the two components of the CME cores, and understand the three-part structure whether the filament is involved or not. The red solid line depicts the MFR boundary in each panel.

As we suggest that the MFR and filament correspond to different parts of the bright core, the three-part structure in this event cannot be explained by the traditional opinion, which regards the MFR and filament as the DC and bright core, respectively, as shown in Figure 6(a) where the red circle depicts the MFR boundary. As mentioned, Howard et al. (2017) and Song et al. (2017b) have demonstrated that the filament-unrelated CMEs can also exhibit the three-part structure, and they propose that the MFR can be observed as the bright core and the cavity is the manifestation of a low-density zone (will be discussed later) between the MFR and BF as presented in Figure 6(b1), where the core is showed with a weaker brightness compared to that in Figure 6(a). The MFR will grow/expand during the propagation outward and the original cavity region will reduce as displayed in Figure 6(b2). Figure 5 in Song et al. (2017b) demonstrates this process with LASCO observations. For the present event, we propose that the MFR and filament correspond to the fuzzy (gray) and sharp (white) bright core components, respectively, and the cavity can be attributed to a low-density zone as well (Figure 6(c1)). This can reconcile the traditional and new opinions on the nature of the CME cores, and explain the core whether the filament is involved or not. Similarly, the MFR will grow/expand during the propagation and the cavity region will reduce, while the filament material keeps relatively concentrated, as shown in Figure 6(c2).

4. Discussion

As the density of MFR is much lower compared to that of the filament in the corona, the brightness of the filament core is significantly larger than that of the MFR core in the coronagraph (Figure 4(g)). If the sensitivity of the coronagraph is not high enough, we may be unable to distinguish the FC between the SC (filament) and DC, and both the FC (MFR) and DC (low-density zone) in Figure 6(c1) might be observed as the DC. In this case, the MFR is taken as one part of the DC and the filament is regarded as the unique bright core, close to the traditional explanation on the three-part structure. The large density difference between the filament and MFR should be one crucial factor that prevents us from noticing the fuzzy component. Alternatively, if the MFR (hosting filament) grows/expands quickly in the beginning stage of the eruption, i.e., the situation as shown in Figure 6(c2) appears in the very low corona, the three-part structure might be explained with the traditional scenario (Figure 6(a)) and we will not be able to observe the FC either. As mentioned, the FC is not easy to distinguish in the COR1 images for this event (see Figure 3), which might be due to the relatively lower sensitivity of COR1 and/or the projection influence of complex foreground and background structures in the low corona. More three-part CMEs containing both the sharp and FC components are expected with higher-sensitivity coronagraphs in the future.

The substantial evidence, which can identify a coronal structure as an MFR, should be based on the magnetic field measurements. Unfortunately, the reliable observations of coronal magnetic fields are not yet available. Therefore, we cannot conclude that the FC has the helical magnetic field structure, i.e., corresponding to the MFR. However, considering its location relationship with the filament, its growth/expansion during propagation, the CME theories (e.g., Chen 2011), and previous studies (Howard et al. 2017; Song et al. 2017b), no obvious conflictions with theories and other observations exist if we suggest that the FC corresponds to the MFR structure. Each observational characteristic of the three-part CMEs can be explained with a uniform scenario as illustrated in Figure 6(c1) whether the filament is involved or not.

It is inevitable to discuss the nature of the DC if both the filament and MFR correspond to the CME core. The CME simulations demonstrate that the MFR usually cannot fill the entire space below the overlying loops during its onset (e.g., Antiochos et al. 1999; Lynch et al. 2008; Fan 2016), consistent with the observations, which show that a low-density zone often exists between the MFR and overlying loops in the early stage of the eruption (see Figure 1 of Song et al. 2014b). This zone could be observed as the cavity in the low corona with coronagraph. The cavity (low-density zone) cannot exist for a long period and will be transformed into the shell part of the MFR through reconnection when propagating outward (e.g., Zuccarello et al. 2012). In the meantime, as the MFR is not in pressure balance with its background near the Sun, the expansion can play an important role in its evolution. Both the expansion and reconnection can lead to the increase of the MFR volume, and substantial differences exist between the two processes, i.e., the expansion maintains the magnetic flux constant and the reconnection adds new flux to the MFR. However, it is not easy to distinguish which process contributes dominantly to the volume increase only based on the image observations. More detailed observational analyses and simulations are necessary to address this issue. A recent study demonstrates one possible mechanism that can form the low-density zone, which shows that a rising electric current in the core

(MFR and/or filament) can induce an oppositely directed electric current in the background plasma. The magnetic force between the two currents propels the background plasma away from the core, creating the low-density zone, and density pileup at the zone edge (Haw et al. 2018). This provides one possible explanation for the formation of both the DC (low-density zone) and BF (high-density pileup) simultaneously, while noting that its validity on the Sun is open as the study is related to a laboratory plasma experiment.

5. Summary

In this paper, an intriguing CME associated with a filament eruption on 2013 September 29 was recorded by multiple white-light coronagraphs on board the *SOHO* and twin *STEREO* from different perspectives. The COR2B observations showed that the CME exhibited the typical three-part structure. A new feature on the CME core is reported, i.e., the core contains both a sharp and a fuzzy bright component. The sharp component stays relatively concentrated during the propagation outward and is identified as the erupted filament, consistent with the traditional opinion on the core, and the fuzzy component exhibits growth/expansion and is suggested to be the MFR, consistent with the recent opinion. Our study can shed more light on the nature of the CME cores, and explain the core whether or not the filament is involved with a uniform scenario.

We thank the anonymous referee for the constructive comments and suggestions which helped to improve the original manuscript considerably. We are grateful to Profs. Peng-Fei Chen and Jun Lin for their valuable discussion. We acknowledge the use of data from the *SDO*, *SOHO*, and *STEREO* missions. This work is supported by the Shandong Provincial Natural Science Foundation (JQ201710), NSFC grants U1731102, U1731101, 41331068, 11790303, and 11790300, and CAS grants XDA-17040505 and XDA-15010900. X. C. is funded by NSFC grant 11722325.

ORCID iDs

H. Q. Song https://orcid.org/0000-0001-5705-661X

References

Antiochos, S. K., Devore, C. R., & Klimchuk, J. A. 1999, ApJ, 510, 485
Aulanier, G., Janvier, M., & Schmieder, B. 2012, A&A, 543, A110
Brueckner, G. E., Howard, R. A., Koomen, M. J., et al. 1995, SoPh, 162, 357
Chen, J. 1996, JGR, 101, 27499
Chen, P. F. 2009, ApJL, 698, L112
Chen, P. F. 2011, LRSP, 8, 1
Cheng, X., Ding, M. D., Zhang, J., et al. 2014, ApJL, 789, 93
Cheng, X., Zhang, J., Ding, M. D., Liu, Y., & Poomvises, W. 2013, ApJ, 763, 43
Cheng, X., Zhang, J., Liu, Y., & Ding, M. D. 2011, ApJL, 732, L25
Fan, Y. H. 2016, ApJ, 824, 93
Forbes, T. G. 2000, JGR, 105, 23153
Gopalswamy, N., Shimojo, M., Lu, W., et al. 2003, ApJ, 586, 562
Gosling, J. T., McComas, D. J., Phillips, J. L., & Bame, S. J. 1991, JGR, 96, 7831
Gou, T. Y., Liu, R., Kliem, B., Wang, Y. M., & Veronig, A. M. 2019, SciA, 5, eaau7004
Haw, M. A., Wongwaitayakornkul, P., Li, H., & Bellan, P. M. 2018, ApJL, 862, L15
Howard, R. A., Moses, J. D., Vourlidas, A., et al. 2008, SSRv, 136, 67
Howard, T. A., DeForest, C. E., Schneck, U. G., & Alden, C. R. 2017, ApJ, 834, 86
Illing, R. M. E., & Hundhausen, A. J. 1985, JGR, 90, 275
Kazachenko, M. D., Lynch, B. J., Welsch, B. T., & Sun, X. D. 2017, ApJ, 845, 49
Kippenhahn, R., & Schlüer, A. 1957, ZA, 43, 36
Lemen, J. R., Title, A. M., Akin, D. J., et al. 2012, SoPh, 275, 17
Lin, J., & Forbes, T. G. 2000, JGR, 105, 2375
Lin, J., Raymond, J. C., & van Ballegooijen, A. A. 2004, ApJ, 602, 422
Linker, J. A., Lionello, R., & Mikić, Z. 2001, JGR, 106, 25165
Lynch, B. J., Antiochos, S. K., Devore, C. R., Luhmann, J. G., & Zurbuchen, T. H. 2008, ApJ, 683, 1192
Lynch, B. J., Antiochos, S. K., MacNeice, P. J., Zurbuchen, T. H., & Fisk, L. A. 2004, ApJ, 617, 589
Mikić, Z., & Linker, J. A. 1994, ApJ, 430, 898
Munro, R. H., Gosling, J. T., Hildner, E., et al. 1979, SoPh, 61, 201
Ouyang, Y., Yang, K., & Chen, P. F. 2015, ApJ, 815, 72
Ouyang, Y., Zhou, Y. H., Chen, P. F., & Fang, C. 2017, ApJ, 835, 94
Patsourakos, S., Vourlidas, A., & Stenborg, G. 2013, ApJ, 764, 125
Reeves, K. K., Linker, J. A., Mikić, Z., & Forbes, T. G. 2010, ApJ, 721, 1547
Song, H. Q., Chen, Y., Qiu, J., et al. 2017a, ApJL, 836, L11
Song, H. Q., Chen, Y., Zhang, J., et al. 2015, ApJL, 808, L15
Song, H. Q., Cheng, X., Chen, Y., et al. 2017b, ApJ, 848, 21
Song, H. Q., Zhang, J., Chen, Y., & Cheng, X. 2014a, ApJL, 792, L40
Song, H. Q., Zhang, J., Cheng, X., et al. 2014b, ApJ, 784, 48
Vourlidas, A., Lynch, B. J., Howard, R. A., & Li, Y. 2013, SoPh, 284, 179
Wang, W. S., Liu, R., Wang, Y. M., et al. 2017, NatCo, 8, 1330
Webb, D. F., Forbes, T. G., Aurass, H., et al. 1994, SoPh, 153, 73
Webb, D. F., & Howard, T. A. 2012, LRSP, 9, 3
Webb, D. F., & Hundhausen, A. J. 1987, SoPh, 108, 383
Wood, B. E., Howard, R. A., & Linton, M. G. 2016, ApJ, 816, 67
Yan, X. L., Priest, E. R., Guo, Q. L., et al. 2016, ApJ, 832, 23
Zhang, J., Cheng, X., & Ding, M.-D. 2012, NatCo, 3, 747
Zhang, J., Dere, K. P., Howard, R. A., & Bothmer, V. 2003, ApJ, 582, 520
Zhang, J., Richardson, I. G., Webb, D. F., et al. 2007, JGR, 112, A10102
Zuccarello, F. P., Bemporad, A., Jacobs, C., et al. 2012, ApJ, 744, 66